New 2D ultrasound phased-array design for hyperthermia cancer therapy

Hasan Sharifi[1] and Hamid Soltanian-Zadeh[1,2]
[1]Electrical and Computer Engineering Department, University of Tehran, Tehran 14399, Iran
[2]Diagnostic Radiology Department, Henry Ford Health System, Detroit, MI 48202, USA

ABSTRACT

We have designed and evaluated (using computer simulations) several different 2D phased arrays with square elements for deep localized hyperthermia. These arrays include a 20x20 planar array, a 80x16 cylindrical-section array, and a 16x16 spherical-section array. Also, we have designed a new phased array with circular elements. We used single and multiple focus scanning methods with intensity gain maximization. We found that the array with circular elements is more effective in reducing grating lobes compared to the same array with square elements. The grating lobes were at least 30 dB smaller than the phased array with square elements and intensity gain was at least 1 dB greater. In addition, with equal intensity distribution patterns for rectangular and circular phased arrays, the number of elements in the circular phased array was smaller and its intensity gain was greater than the other arrays.

keywords: hyperthermia, phased arrays, single-focus scanning, multiple-focus scanning, intensity gain maximization, computer simulation

1. INTRODUCTION

Several modalities are currently used to generate localized hyperthermia, including radio frequency currents, microwaves, and ultrasound. Each has advantages and disadvantages when compared to the others and no one modality is ideal for all clinical treatment situations. Of the two noninvasive modalities that are currently used for localized hyperthermia, ultrasound has a much shorter wavelength than microwave radiation for frequencies used for hyperthermia applications. This represents a strong advantage to the use of ultrasound as opposed to microwaves since the former can be well localized and controlled at depth whereas the latter cannot[1].

The use of phased arrays as heating applicators has several advantages. First, as multiple-transducer applicators, phased arrays can easily compensate for the effects of inhomogeneities of the treatment volume (which includes the tumor and the surrounding tissues). Secondly, the heating pattern can be controlled electronically, thus eliminating the need for mechanical movement of the applicator head. This simplifies the machine patient interface and allows for better use of the available acoustic windows. Thirdly, electronic switching can be performed rapidly, thus enabling swift response to changes in the tumor environment. Fourthly, phased arrays can be used to directly synthesize multiple-focus field patterns, which can be scanned to produce the desired time-average power deposition pattern. This approach is referred to as multiple-focus scanning.

Direct synthesis of heating patterns is advantageous in reducing the spatial-peak temporal-peak intensity required to produce the desired time-average heating pattern. This might be necessary to avoid certain non-linear phenomena associated with high-intensity ultrasound, e.g., intensity saturation[2,3] and transient cavitation[4]. Simulation results presented in reference[3] for spherically focused transducers with Gaussian beam profiles indicate that non-linear propagation can enhance the power deposition in the treatment volume. This is due to the fact that non-linear wave propagation is associated with the generation of higher-order harmonics, which have higher absorption coefficients. The enhancement in power deposition depends on several factors, e.g., absorption, initial cross-section of the wavefront, and focal depth. It should be noted, however, that this enhancement in power deposition can be achieved only at certain focal intensity levels. The opposite effect can occur when much higher focal intensity levels are attempted. In such cases, higher-order harmonics will be absorbed in the intervening tissue before reaching the focus (intensity saturation). The general conclusion of the simulation study performed in reference[3] is that there exist optimal focal intensity levels at which non-linear wave propagation can be used to enhance the power deposition in the tumor volume. Therefore, direct synthesis of multiple-focus field patterns can be useful not only in avoiding intensity saturation, but also in enhancing the power deposition in the tumor by operating at the optimal focal intensity level. A more serious potential problem associated with high-intensity focused ultrasound is transient cavitation[4]. Transient cavitation has been detected at intensity levels as low as $67 W/cm^2$ at a frequency of 386 kHz in pork muscle using continuous wave (CW) ultrasound[5]. To avoid cavitation at frequencies as low as 500 kHz, Hynynen[6] suggested the use of non-overlapping multiple-beam heating patterns to spread the ultrasonic energy spatially while reducing the spatial-peak intensity to levels well below the cavitation threshold. This can be achieved by multiple-focused transducers[7], specially fabricated lens-focused transducers[8,9] or phased-array applicators. The latter approach offers most flexibility in terms of applicator size and adaptive control of the heating patterns. However, one disadvantage of multiple-focus field synthesis is possible formation of high-intensity interference patterns outside the target volume, which might lead to hot spots in normal tissues surrounding the tumor.

The direct synthesis of multiple-focus field patterns with phased arrays can be achieved using the pseudo-inverse method. This method finds the minimum-energy excitation vector (of complex particle velocities at the surfaces of array elements), which produces specified power deposition levels at a set of selected points in the treatment volume (called control points)[10].

2. METHODS

The phases and amplitudes of driving signals at the NxN array elements (Fig. 1) required to produce single focus or multiple-focus absorbed power distributions are determined using the pseudo-inverse method[10]. The pressures P_m at M control points are obtained by summing the contributions from each of the elements, i.e.,

$$P_m(r_m) = \frac{j\rho c}{\lambda}\sum_{n=1}^{N} u_n \int_{S_n} \frac{e^{-jk|r_m - r_n|}}{|r_m - r_n|} ds_n \qquad (1)$$

where m=1, 2,…M and ρ, C, $k = (2\pi/\lambda + j\alpha)$ are the density (10^3 kg/m^3), speed of sound (1500 m/s) and propagation constant in the medium, respectively, λ is the wavelength, α, the attenuation, is taken to be 1 dB/cm/MHz, s_n and u_n are the surface area and the complex surface velocity of the n*th* element, r_m and r_n are the positions of the m*th* control point and n*th* element, and P_m is the desired pressure at the m*th* control point.

Taking

$$\frac{j\rho c}{\lambda} \int_{s_n} \frac{e^{-jk|r_m - r_n|}}{|r_m - r_n|} ds_n = h_{mn}, \qquad (2)$$

we can write

$$H_M U_M = P_M \qquad (3)$$

where H_M is an MxN matrix with elements h_{mn} (the forward propagation operators), U_M is the vector of the N complex velocities at the surface of the elements, and P_M is the vector of the M complex pressures at the control points. Since in these simulations, M<N, the required complex velocities are obtained from

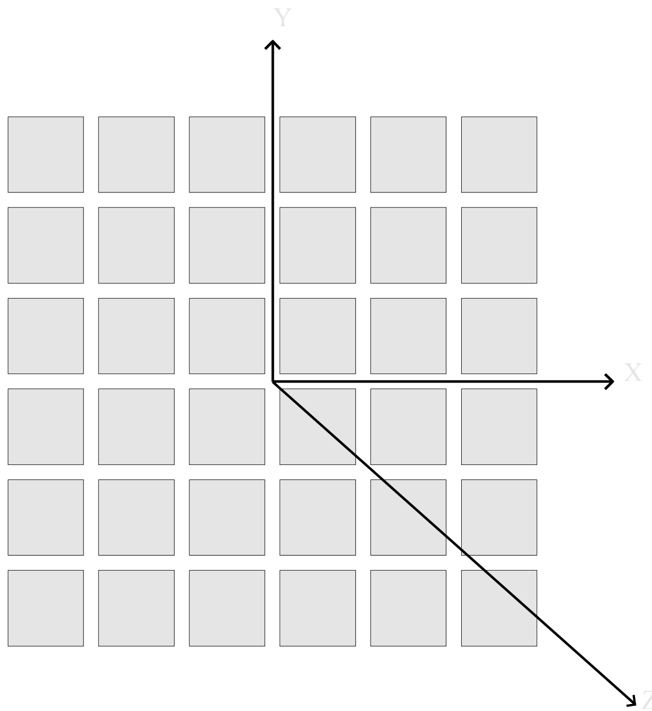

(a)

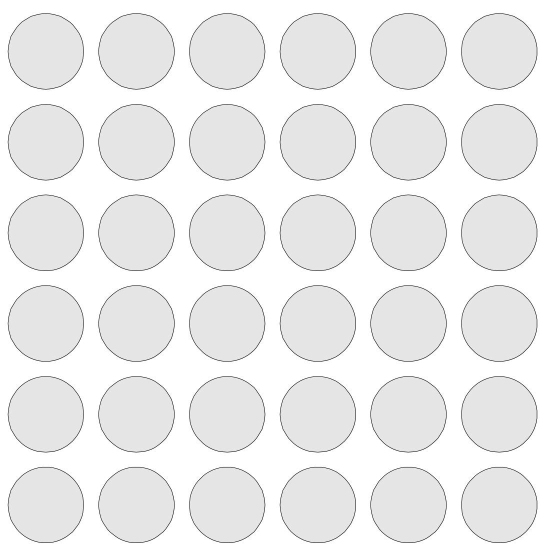

(b)

Fig. 1.a,b. Schematics of phased arrays with square element applicators (a) and with circular element applicators (b).

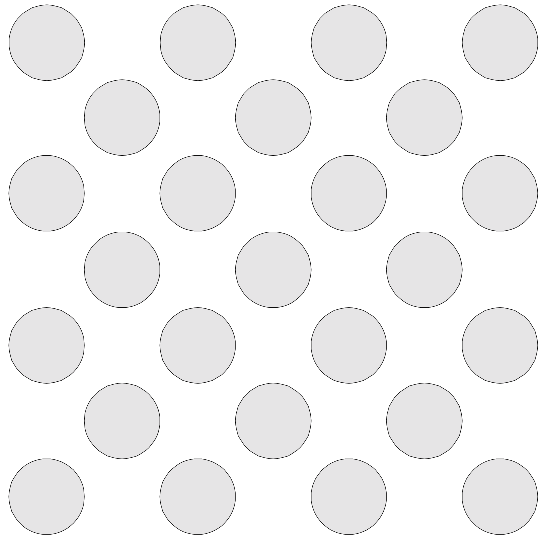

(c)

Fig. 1.c. Schematics of a phased array with circular element applicators.

$$U_M = H_M^{*T}(H_M \cdot H_M^{*T})^{-1} P_M \tag{4}$$

where * and T represent conjugate and transpose, respectively.

Having determined the desired U_M, the pressure field due to the ultrasound array is calculated at the nodes of a 3-dimensional (3D) grid (with inter-node spacing of 1mm) by numerical evaluation of the Rayleigh-Sommerfeld diffraction integral[11,12]. The surface of the array is modeled by small square or circular sub-elements. For each field point (position r), the contributions from such sub-elements covering a single array element are summed in an analogous manner to equation (2) to obtain an array of complex forward propagation operators associated with that element. Then, assuming that all array elements are similar, we use the principle of superposition to obtain P at each nodal point in the field using

$$P(r) = \sum_{n=1}^{N} u_n \cdot h_n(r) \tag{5}$$

where h_n is the appropriate forward propagation operator[13].

There exist several efficient algorithms for evaluating equation (4). The vector P_m specifies the complex pressures at the control points. Our interest, however, is in the power deposition at these points rather than the complex pressures. Since the power deposition is a phase-insensitive quantity, we are free to choose any phase values of the complex pressures at the control points. One would naturally be interested in finding the phase distribution that is optimum in some sense. We choose the phase distribution that maximizes the intensity gain at the control points, defined as equation (6), which is a measure of energy concentration at the control points.

$$G=\frac{P^{*T}P}{U^{*T}U}=\frac{\sum_{m=1}^{M}|p_m|^2}{\sum_{n=1}^{N}|u_n|^2} \tag{6}$$

Substituting for U by the minimum-norm solution in (4), we obtain

$$G=\frac{P^{*T}P}{P^{*}\left(H\cdot H^{*T}\right)^{-1}P} \tag{7}$$

A direct solution to this problem is given in reference[14]. Any enhancement in intensity gain obviously increases the heating efficacy of the phased-array applicators. More significantly, maximization of this quantity was shown to be effective in removing undesired interference patterns from the synthesized field, thus eliminating one of the major problems of direct synthesis of multiple-focus field patterns. Furthermore, this technique significantly reduces the pre-focal-depth high-temperature heating associated with single-focus scanning of deep-seated tumors[15].

3. SIMULATION STUDIES

We used computer simulations to illustrate and evaluate the proposed method. Here, we present simulations done for a 20x20 array with 5x5mm square elements (Fig. 1.a), a 20x20 array with circular elements each having a radius of 2.5mm (Fig. 1.b), and a 14x14+13x13 array with circular elements each having a radius of 3.5mm (Fig. 1.c).

Figs. 2 and 2' show intensity profiles in the X direction at Z = 100mm (focal point) and in the plane Y = 0, respectively. A comparison of the three profiles shows that with equal intensities at the control point, the grating lobes in array (c) are the smallest. Also, gain intensity in array (c) is at least 1dB greater than that of array (a) and 0.5 dB greater than that of array (b). Fig. 3 compares intensity profiles in the Z direction. This Figure illustrates that the profiles of these arrays in the Z direction are approximately the same.

Fig. 4 shows intensity profiles of a multiple-focus array in the X direction at Z = 100mm (focal points). Focal points are located on a circle with a radius of 10mm. Grating lobes in array (c) are the smallest of all arrays. Also, intensity gain in this array is the greatest of all arrays. Table 1 lists intensity gains and grating lobes of the arrays.

Table 1. Arrays Characteristics.

	Array (a)	Array (b)	Array (c)
Number of Elements	400	400	365
Relative Intensity Gain	0 dB	0.5 dB	1 dB
Grating Lobes	-6.9 dB	-10 dB	-17 dB

4. SUMMARY AND CONCLUSIONS

The computer simulation results which have been illustrated in Figs. 2, 3, 4, and Table 1 demonstrate the capability of phased arrays with circular elements for producing diffuse intensity profiles suitable for tumor heating. It is shown that grating lobes in phased arrays that have been designed with circular elements are smaller than those with square elements. In addition, with equal intensity distribution patterns in focal points for rectangular and circular phased arrays, the number of elements in the circular phased arrays is smaller and its intensity gain is greater than the other arrays. In this research, tissue was considered homogeneous, but in practice, it is inhomogeneous. This will be considered in the future work.

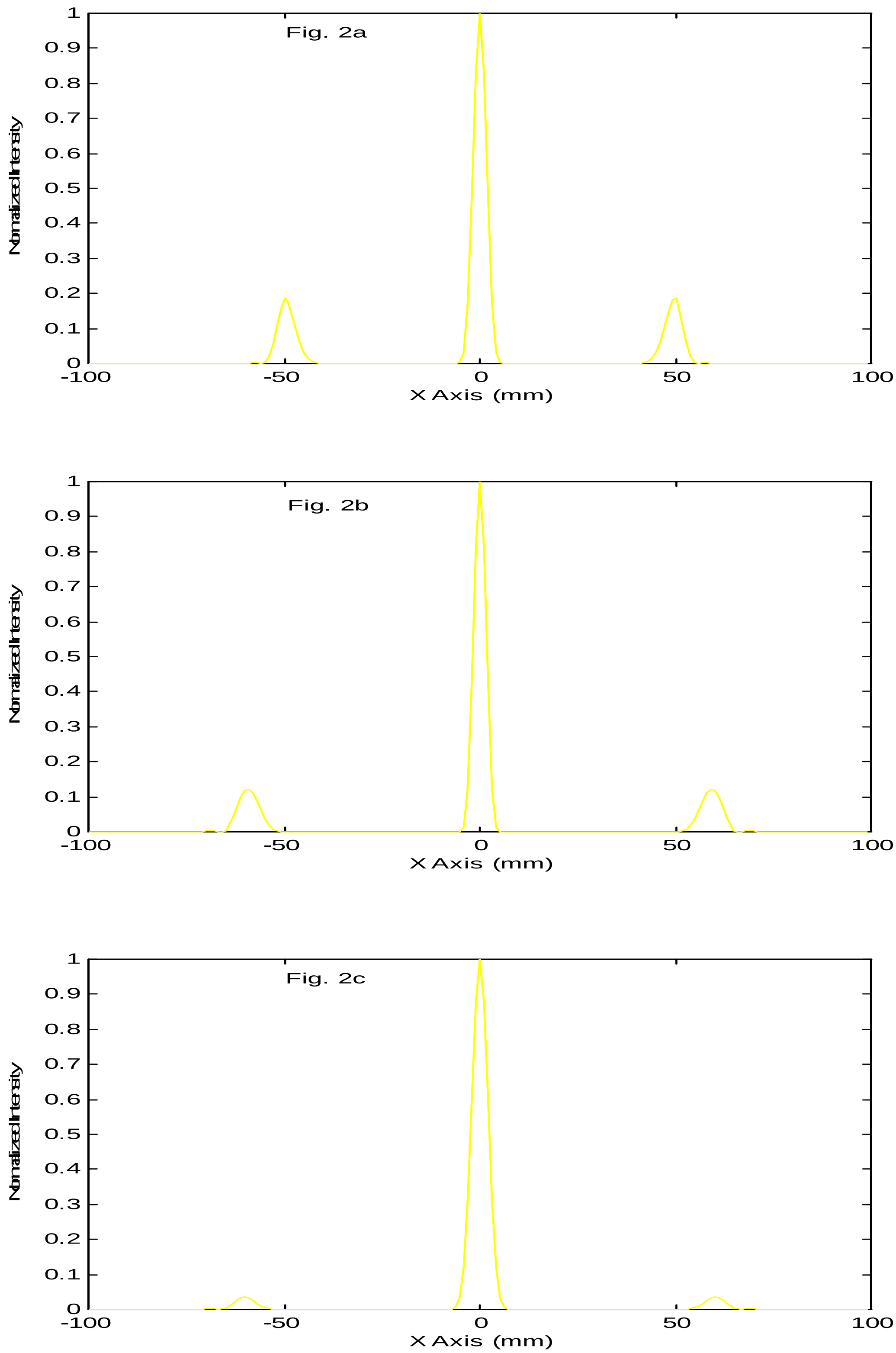

Fig. 2. Intensity profiles of single focus in the X direction at Z = 100mm. (a) for array in Fig. 1.a, (b) for array in Fig. 1.b, (c) for array in Fig. 1.c.

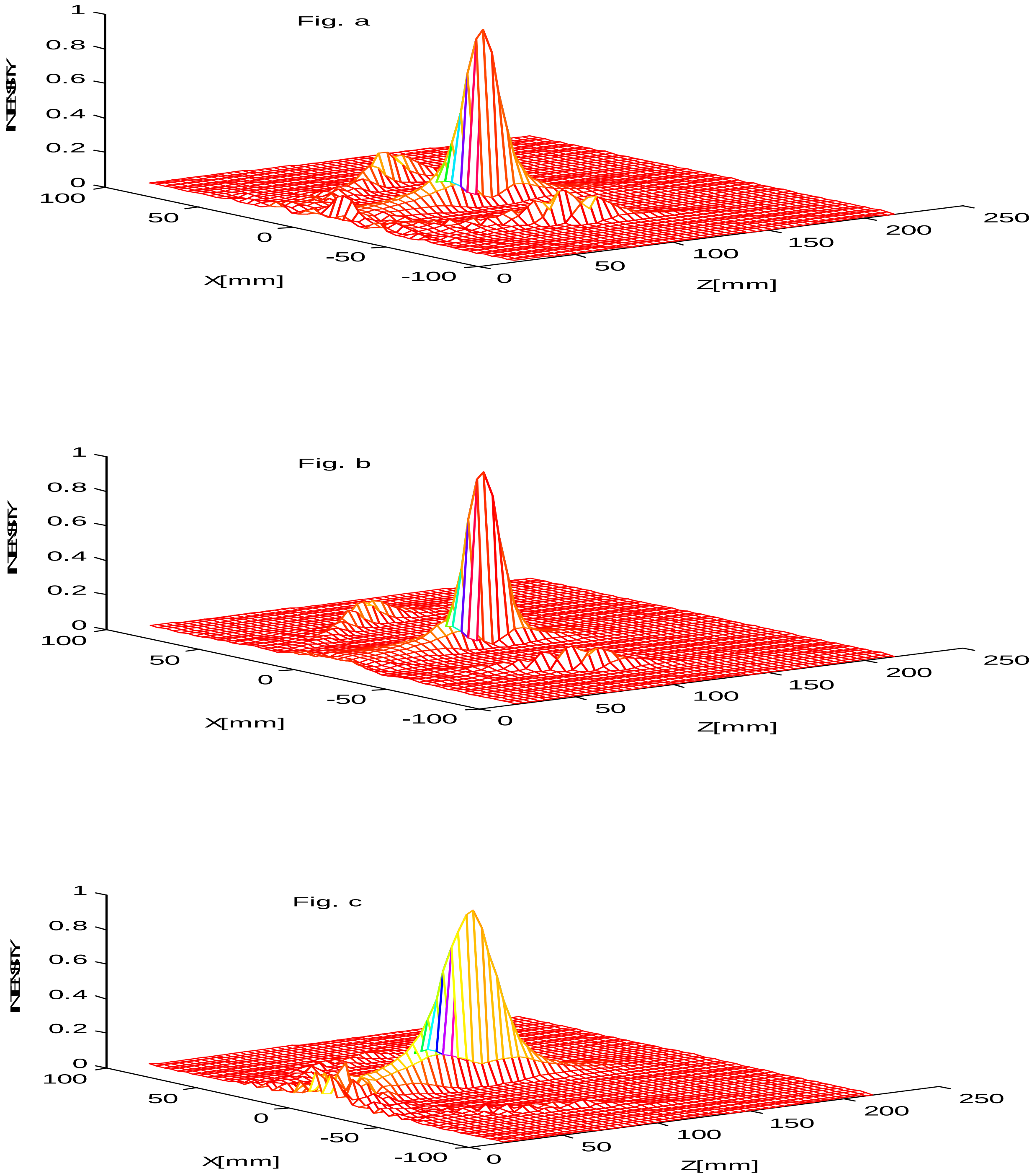

Fig. 2'. Intensity profiles of single focus arrays in a longitudinal plane defined by Y=0. (a) for array in Fig. 1.a, (b) for array in Fig. 1.b, (c) for array in Fig. 1.c.

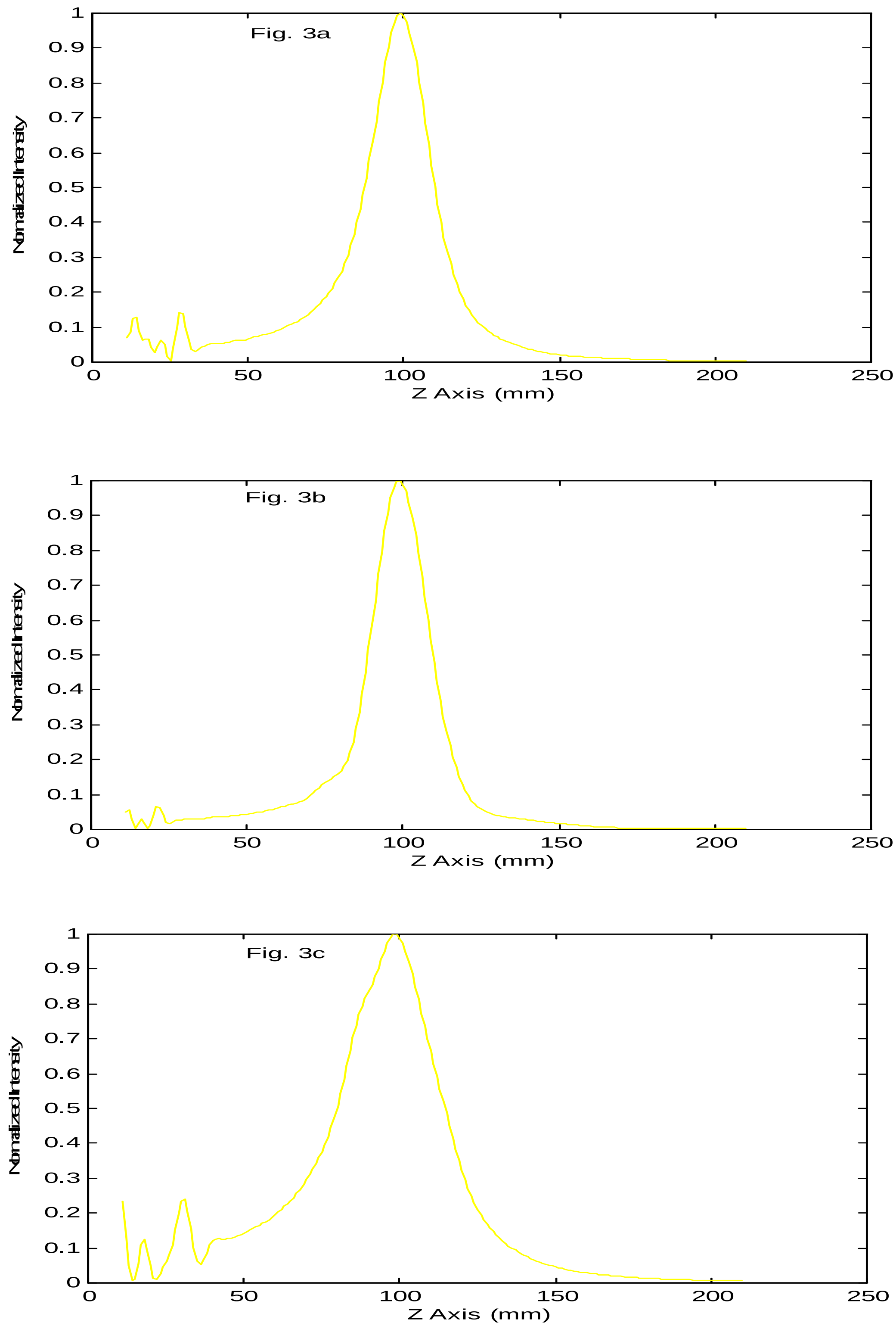

Fig. 3. Intensity profiles of single focus arrays in the Z direction. (a) for array in Fig. 1.a, (b) for array in Fig. 1.b, (c) for array in Fig. 1.c.

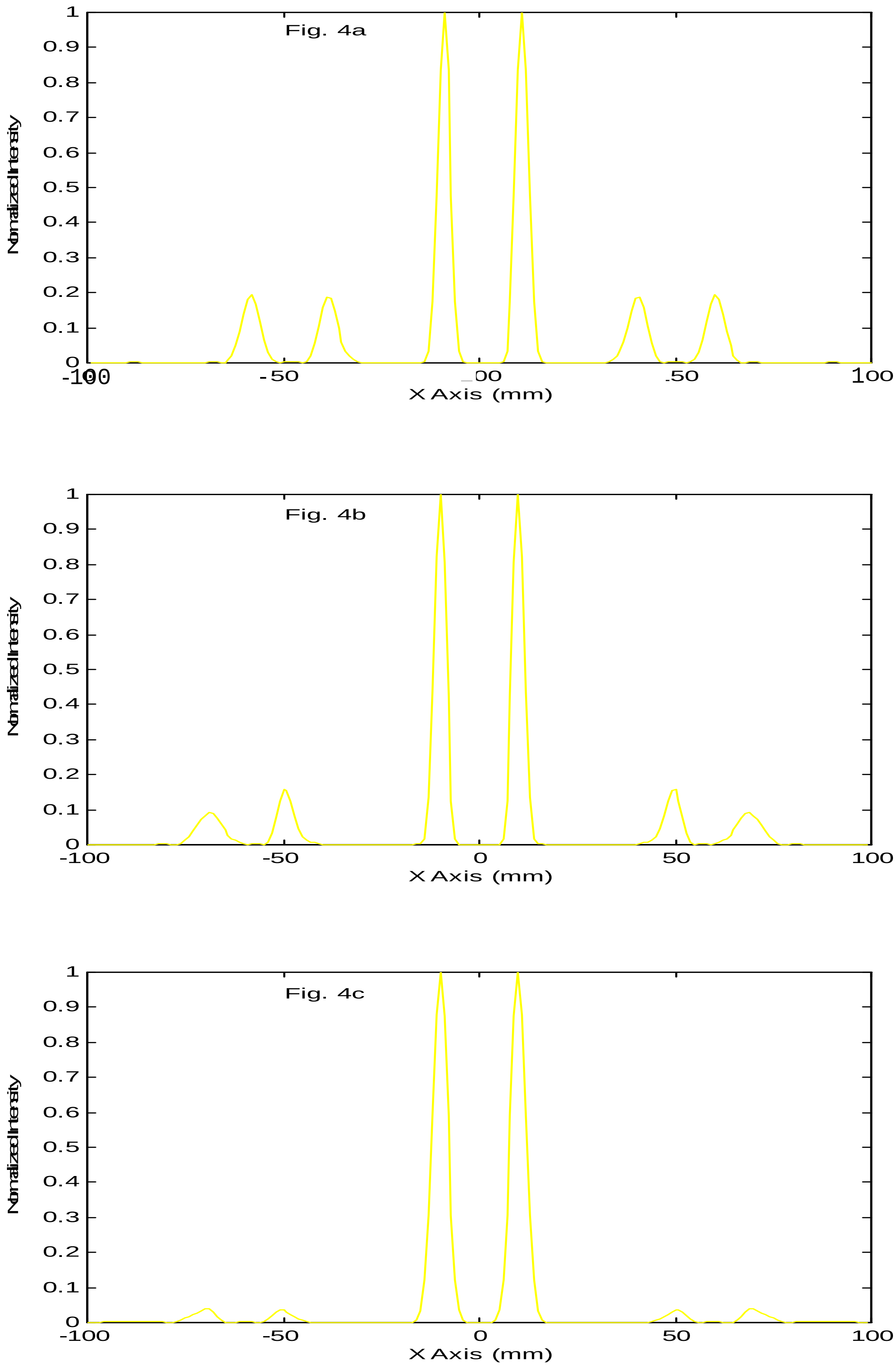

Fig. 4. Intensity profiles of a four-focus array in the X direction at Z = 100mm. (a) for array in Fig. 1.a, (b) for array in Fig. 1.b, (c) for array in Fig. 1.c.

REFERENCES

1. L. A. Frizzell, P. J. Benkeser, K. B. Ocheltree, and C. A. Cain, "Ultrasound Phased Arrays for Hyperthermia Treatment," *Proc. IEEE, Ultrasonics Symposium,* pp. 930-935, 1985.

2. E. Carstensen, W. Law, and D. Mckay, "Demonstration of Nonlinear Acoustical Effects at Biomedical Frequencies and Intensities," *Ultrasound in Medicine and Biology,* vol. 6, pp. 359-368, 1980.

3. W. Swindell, "A Theoretical Study of Nonlinear Effects with Focused Ultrasound in Tissues: A Acoustic Bragg Peak," *Ultrasound in Medicine and Biology,* vol. 11, pp. 121-130, 1985.

4. P.P. Lele, "Effects of Ultrasound on Solid Mammalian Tissues and Tumors in Vivo," *Ultrasound: Medical Applications, Biological Effects and Hazard Potential,* Edited by M. Repacholi, M. Granolfo, and A. Rindi, New York: Plenum Press, pp. 275-306, 1987.

5. F.G. Sommer, and D. Pounds, "Transient Cavitation in Tissues during Ultrasound Induced Hyperthermia," *Medical Physics,* vol. 9, no. 1, pp. 1-3, 1982.

6. K. Hynynen, "The Threshold for Thermally Significant Cavitation in Dog's Thigh Muscle in Vivo," *Ultrasound in Medicine and Biology,* vol. 17, pp. 157-169, 1991.

7. K. Hynynen, R. Roemer, D. Anhalt, C. Johnson, Z.X. Xu, W. Swindell, and T. Cetas, "A Scanned, Focused, Multiple Transducer Ultrasonic System for Localized Hyperthermia Treatments," *International Journal of Hyperthermia,* vol. 3, no. 1, pp. 21-35, 1987.

8. P. Lele, "Physical Aspects and Clinical Studies with Ultrasonic Hyperthermia," *Hyperthermia in Cancer Therapy,* F. C. Storm, Ed., Boston: Hall Medical Publisher, pp. 333-367, 1983.

9. R.J. Lalonde, A. Worthington, and J.W. Hunt, "Modelling Temperature Distributions Produced by Ultrasound Phased Arrays for Hyperthermia," *Proceedings of IEEE Ultrasonics Symposium,* vol. 2, pp. 941-944, 1989.

10. E. Ebbini, C. A. Cain, "Multiple-Focus Ultrasound Phased Array Pattern Synthesis: Optimal Driving Signal Distributions for Hyperthermia," *IEEE Trans. Ultrason. Ferroelec. Freq. Contr.,* vol. 36, no. 5, pp. 540-548, 1989.

11. Kenneth B. Ocheltree, and Leon A. Frizzell, "Sound Field Calculation for Rectangular Sources," *IEEE Trans. Ultrason. Ferroelec. Freq. Contr.,* vol. 36, no. 2, pp. 242-248, 1989.

12. J. Zemanek, " Beam Behavior within the Nearfield of a Vibrating Piston," *J. Acoust. Soc. Am.,* vol. 49, no. 1, pp. 181-191, 1971.

13. J. W. Hand, E. Ebbini, D. O'Keeffe, D. Israel, and S. Mohammadtaghi, "An Ultrasound Linear Array for Use in Intracavitary Applicators for Thermotherapy of Prostatic Diseases," *Proc. IEEE, Ultrasonics Symposium,* pp. 1225-1228, 1993.

14. E. Ebbini, and C. A. Cain, "Optimization of the Intensity Gain of Multiple-Focus Phased-Array Heating patterns," *Int. J. Heperthermia,* vol. 7, no. 6, pp. 953-973, 1991.

15. E. Moros, R. Roemer, and K. Hynynen, "Pre-focal Plane High-temperature Regions Induced by Scanning Focused Ultrasound Beams," *International Journal of Hyperthermia,* vol. 6, pp. 351-366, 1990.